

УДК 551.465

© В. Г. Гневнышев¹, А. В. Фролова², А. В. Колдунов², Т. В. Белоненко^{2*}

© Перевод Е.С. Кочеткова, 2021

¹Институт океанологии им. П.П. Ширшова РАН, 117997, Нахимовский пр., д. 36, г. Москва, Россия

²Санкт-Петербургский государственный университет, 199034, Университетская наб., 7–9,

г. Санкт-Петербург, Россия

*E-mail: btvlisab@yandex.ru

ТОПОГРАФИЧЕСКИЙ ЭФФЕКТ ДЛЯ ВОЛН РОССБИ НА ЗОНАЛЬНОМ СДВИГОВОМ ПОТОКЕ

Статья поступила в редакцию 19.08.2020, после доработки 23.11.2020

Проводится сравнительный анализ влияния топографии, β -эффекта и градиента меридиональной изменчивости фонового течения на распространение баротропных топографических волн Россби. Опираясь на уже полученные результаты о том, что короткие волны практически не наблюдаются, а также учитывая, что влияние стратификации на длинные волны Россби незначительно, мы исключаем из задачи влияние стратификации и рассматриваем вертикально интегрированное зональное течение. Меридиональную изменчивость фонового течения топографии мы рассматриваем в ВКБ-приближении. Это позволяет получить дисперсионное соотношение для плоских баротропных топографических волн Россби, в котором одновременно учитываются эффекты, связанные с вращением Земли, сдвиг скорости и топография. В рассмотренных примерах сдвиг скорости течения рассчитывается по данным продукта GLORYS12v1 для акватории расположенного в зоне действия Антарктического циркумполярного течения. В качестве топографической структуры рассматривается зонально вытянутый хребет, рельеф которого аппроксимируется экспонентой или гауссианой с различными параметрами. Установлено, что локально вклад сдвигового течения может перекрывать вклад топографии. Показано, что топографический фактор в дисперсионном соотношении является доминирующим, при этом с северной стороны хребта в южном полушарии топография усиливает действие β -эффекта, а с южной стороны — ослабляет.

Ключевые слова: Волны Россби, ВКБ-приближение, дисперсионное соотношение, нелинейные эффекты, топография, струйное течение, Антарктическое циркумполярное течение, АЦТ, GLORYS12v1.

© V. G. Gnevyshev¹, A. V. Frolova², A. V. Koldunov², T. V. Belonenko^{2*}

© Translation E.S. Kochetkova, 2021

¹Shirshov Institute of Oceanology RAS, 117997, Nahimovsky Pr., 36, Moscow, Russia

²St. Petersburg State University, 199034, 7–9, Universitetskaya Emb., St. Petersburg, Russia

*E-mail: btvlisab@yandex.ru

TOPOGRAPHIC EFFECT FOR ROSSBY WAVES ON A ZONAL SHEAR FLOW

Received 19.08.2020, in final form 23.11.2020

The present study analyses the influence of topography, β -effect, and the gradient of the meridional variability of the background current on the barotropic topographic Rossby waves. We exclude the stratification effect from the problem and consider a vertically integrated zonal flow because the previous results show that short waves are seldom, and the stratification effect on long Rossby waves is insignificant. We consider the transverse (meridional) variability of the background topography current in the WKB approximation. Thus, we obtain a dispersion relation for plane barotropic topographic Rossby waves, which simultaneously accounts for the effects of the Earth's rotation, velocity shear, and topography. The GLORYS12v1 product for the Antarctic Circumpolar Current zone is used to calculate the current velocity shift. The topography structure is modeled as an elongated ridge and approximated by an exponential and a Gaussian function with different parameters. The results show that the contribution of the shear flow can overlap the contribution of topography locally. The topographic factor in the dispersion relation is dominant. Specifically, in the southern hemisphere, on the northern side of the ridge, the impact of topography on the Rossby waves intensifies due to the β -effect, while, on the southern side, it reduces due to the β -effect.

Key words: Rossby waves, WKB approximation, dispersion relation, nonlinear effects, topography, jet flow, Antarctic Circumpolar Current, ACC, GLORYS12v1

Ссылка для цитирования: Гневнышев В.Г., Фролова А.В., Колдунов А.В., Белоненко Т.В. Топографический эффект для волн Россби на зональном сдвиговом потоке // *Фундаментальная и прикладная гидрофизика*. 2021. Т. 14, № 1. С. 4–14. doi: 10.7868/S2073667321010019

For citation: Gnevyshev V.G., Frolova A.V., Koldunov A.V., Belonenko T.V. Topographic Effect for Rossby Waves on a Zonal Shear Flow. *Fundamentalnaya i Prikladnaya Gidrofizika*. 2021, 14, 1, 4–14. doi: 10.7868/S2073667321010019

1. Introduction

Established that, in the propagation of Rossby waves in the ocean, the key role belongs to the relationship between the meridional heterogeneity of the Coriolis parameter (β -effect) and topographic changes in the relief. If we simultaneously take into account the large-scale topographic variability in the bottom topography and the differential rotation of the Earth, then the generalized parameter β , including both factors, is determined by the relation [1]:

$$\beta^* = -\frac{f^2}{H} \frac{\partial(H/f)}{\partial y} = \frac{\partial f}{\partial y} - \frac{f}{H} \frac{\partial H}{\partial y}.$$

From this formula it follows, that the propagation of Rossby waves is influenced simultaneously by meridional changes in the Coriolis parameter f and meridional changes in depth H . Enstrophy conservation requires compensation of the planetary-topographic vorticity by the intrinsic vorticity of planetary waves, and, as the fluid particles move through the contours $\frac{f}{H}$, their relative vorticity also changes. Consequently, an increase in the planetary wave effects is expected where there is a thickening of isolines $\frac{f}{H}$, for example, near the mid-ocean ridges [2]. The influence of topographic features on the propagation of barotropic planetary waves was first considered by Veronis [3] and Rhines [4]. See please other research in papers [5–7].

In recent years, emerging studies analyze the background baroclinic flow influence on the propagation of planetary waves. The mean flow changes the potential vorticity waveguide in which waves propagate, and the velocity shear contributes to the vorticity balance. Bobrovich and Reznik [8] analyze a one-parameter asymptotic expansion for a continuous stratification problem. The authors consider linear Rossby waves in a continuously stratified ocean with a rough bottom and show that for the case of a constant buoyancy frequency, but without taking into account the current, there are three types of regimes: topographic regime, barotropic regime, and a discrete set of baroclinic regimes (see also [9]).

Continuing these investigations, Gnevyshev et al. [10] show that Rossby waves propagating in the waveguide interact nonlinearly with the flow, and the Doppler shift is balanced by nonlinearity. Using altimetry data for the Antarctic Circumpolar Current (ACC), the authors demonstrate that meridional changes in planetary vorticity can be counterbalanced by local meridional changes in relative vorticity. In this case, in the expression for β^* , which is «effective» β , the meridional gradient of the zonal velocity shear prevails U_{yy} : $\beta^* = \beta - U_{yy}$, where $\beta = \frac{df}{dy}$, as a result, Rossby waves in the ACC waveguide can propagate eastward [10]. However, in areas of jet streams, large-scale topographic features also affect the dynamics of Rossby waves. A comparative contribution of the Earth differential rotation, a shear flow, as well bottom topography to the equation of conservation of a potential vortex has not been estimated previously. In this paper, we study the influence of these factors on the propagation of Rossby waves in several ACC regions, both with model situations and according to oceanic reanalysis data. Analyzing the topography effect, we believe that the topography is zonally homogeneous. In this work, we do not consider such phenomena as, for example, the resonant response from the passage of waves over a meridionally homogeneous ridge of hills. These problems are more typical of the atmosphere than of the ocean.

The initial problem formulation for the joint influence of topography and stratification is outlined by Rhines [4]. The author discusses a regime with steep slopes when the node of the first baroclinic mode shifts to the bottom. Rhines concludes that with an increase in the bottom slope and the wavenumber increase (decrease in the wavelength), the near-surface wave changes its vertical mode and, instead of the near-surface one, becomes a bottom-trapped mode. This influence of topography on short Rossby waves sometimes is interpreted as a topographic filter in the propagation of short Rossby waves. Perhaps, due to the topographic filter, hardly any short waves are recorded in observations during field observations. It is important to note that, depending on the bottom slope, topography can either enhance or weaken the β -effect.

In the general case, when stratification, topography, and β -effect are simultaneously present, the variables are not separated, and the problem becomes analytically complicated. Therefore, starting with the work of Rhines, the influence of topography and stratification or topography and the β -effect [11] are analyzed separately. These considerations lead to approximations known in the literature as the first and second Rhines approximation [2]. The current state of the art of formulation of this problem in terms of “topography plus stratification” can be found in the study [12]. In addition to numerical calculations’ results in this formulation, the particular solution with Bessel functions is an undoubted success that helps circumvent solving the transcendental eigenvalue equation.

Despite significant improvements in the agreement between theory and observed data, the listed works have not provided anything qualitatively new since Rhines. In particular, Brink & Pedlosky [13], in addition to surface pumping, modified the lower boundary condition by adding bottom friction. The introduction of bottom friction complicates the problem even in a linear setting because it introduces instability to the problem. The vertical problem numerical solution with actual stratification, velocity field, and topography in specific regions of the World Ocean was performed [14, 15]. The authors showed that taking into account baroclinicity and actual stratification, numerous problems arise, up to the absence of neutral modes as such. Note that, based on the presented numerical calculations, the authors conclude that the seasonal change in the stratification field is not significant for the analysis of the eigenvalue problem and thus, use the average annual stratification field.

We follow the works of Gill [16] and Chelton et al. [17–18], where they argued that stratification does not affect long waves. The novelty of the present problem formulation is in simultaneous consideration of all three factors that affect Rossby waves, differential rotation of the Earth, shear flow, and topography. Rejecting the traditional linear approach to the dispersion equation and relying on the results already obtained that short waves are practically not observed [12], and also considering that the effect of stratification on long Rossby waves is not so significant [16–18], we exclude the influence of stratification from the problem. Also, to avoid complications with critical layers, we consider a vertically integrated zonal flow to obtain an analytical expression for the phase velocity. We study the transverse (meridional) variability of the topography background current in the WKB approximation and with model topography profiles. This approach allows direct assessment of the contribution of the β -effect, the relative influence of topography, and the gradient of the background current meridional variability.

To apply this approach in practice, we selected an area in the ACC area. The absence of land barriers in the ACC leads to pronounced dynamic features, which direct analogs are not found in the theory of mid-latitude ocean gyres. The main elements of the bottom topography influencing the ACC are the Drake Passage, Kerguelen Plateau, Campbell Plateau, Macquarie Ridge, and the Pacific–Antarctic Ridge. The main barrier directly in the ACC band is the Austral–Antarctic Ridge [19]. The presented elements of the oceanic relief affect both the direction of the current flow and the kinetic energy of the vortices in the flow. Thus, after the flow crosses the underwater ridge, the number of small-scale eddies increases. Even relatively small eddies account for a significant portion of the flow vortex kinetic energy [20]. Also, mesoscale eddies (10–100 km in diameter) can form due to large-scale irregularities in the bottom topography [21], barotropic [22–23], and baroclinic instability of the ACC [24]. The temporal and spatial scales of variability typical for ACC range from 10 to 100 days and 25 to 250 km [25].

Despite the relatively slow flow in the regions between the fronts, the current carries more water than any other ocean current [22]. The ACC transfers a total of 173.3 Sv through the Drake Passage (barotropic transport 45.6 Sv, baroclinic transport equal to 127.7 Sv) [26]. Also, numerous studies confirm the significant influence of bottom topography on flow behavior, which controls ACC jets propagating up to 2000–4000 m in depth [27–29]. Undoubtedly, large-scale topographic structures have a significant impact on the propagation of Rossby waves in the ocean. However, which mechanisms contribute the most remains a mystery, differential rotation of the Earth, shear flow, or topography. For this purpose, we derive a more general dispersion relation for Rossby waves, in which an additional term appears, reflecting the mutual influence of topography and variability of the background jet flow. Further, we consider several analytical topography models, for which we estimate the terms from the new generalized dispersion equation. Thus, a comparative analysis of the contribution of various factors to the linear dispersion equation for Rossby waves is the purpose of this work.

2. Data used

For this work, we used several types of data:

GLORYS12v1, product is available on Copernicus Marine Environment Monitoring Service (CMEMS) portal at <http://marine.copernicus.eu>. It is a vortex-resolving reanalysis based on the NEMO hydrodynamic model of the ocean and the ERA-Interim atmospheric reanalysis. The values of temperature, salinity, current components, level anomalies are distributed on a regular grid on 50 horizons. The spatial resolution of the data is $1/12^\circ$. The indisputable advantage of GLORYS is data assimilation, which assimilates all available contact measurements (data of temperature and salinity profiles from the CMEMS CORAv4.1 database since 2005), and remote sensing data (surface temperatures using the AVHRR radiometer, sea level from all altimeters, etc.). Observations are assimilated using a reduced-order Kalman filter. ERA-interim atmospheric reanalysis is used as forcing. The initial conditions for temperature and salinity were set from EN.4.2.0. Hadley center for 1991. For this study, we used the zonal component of the flow velocity data for the period 01–31.11.2018.

We used the data of the bathymetric product GEBCO_2020, developed within the framework of The General Bathymetric Chart of the Oceans (GEBCO) project (<https://www.gebco.net/>). This data provides global coverage on a grid with a spatial resolution of $1/250^\circ$ in latitude and longitude.

3. Results

3.1. Some theoretical aspects

Rossby waves are gradient vortex waves [30], which means that their propagation is driven by the potential vorticity gradient, for which the conservation law is:

$$\frac{d_h}{dt} \left(\frac{\zeta + f}{H} \right) = 0, \quad (1)$$

where $\frac{d_h}{dt} = \frac{\partial}{\partial t} + U \frac{\partial}{\partial x} + V \frac{\partial}{\partial y}$, x and y are zonal and meridian variables of a rectangular coordinate system, in which the abscissa axis is directed to the east, and the ordinate axis is to the north, t is time, $\zeta = V'_x - U'_y$ is relative vorticity, U and V are zonal and meridional current velocity components, f is planetary vorticity (Coriolis parameter), H is the ocean depth. On the continental shelf, a potential vorticity gradient arises as a consequence of an increase in water depth in a direction perpendicular to large-scale topographic irregularities. We accept the notation used in the monograph by LeBlond & Mysak [2] and assume that the depth increases from the ocean surface towards the bottom.

With the mass stream function:

$$\begin{aligned} HU &= -\Psi_y, \quad HV = \Psi_x, \\ \zeta &= V_x - U_y = \left(\frac{\Psi_x}{H} \right)_x + \left(\frac{\Psi_y}{H} \right)_y. \end{aligned} \quad (2)$$

Then equation (1) takes the form

$$\left[\frac{\partial}{\partial t} - \frac{\Psi_y}{H} \frac{\partial}{\partial x} + \frac{\Psi_x}{H} \frac{\partial}{\partial y} \right] \left[\frac{1}{H} \left\{ \left(\frac{\Psi_x}{H} \right)_x + \left(\frac{\Psi_y}{H} \right)_y + f \right\} \right] = 0. \quad (3)$$

Next, we apply the standard linearization procedure against the background of a stationary zonal flow

$$\Psi(x, y, t) = \Psi_s(y) + \varepsilon \tilde{\Psi}(x, y, t), \quad \varepsilon \ll 1, \quad (4)$$

where $U(y) = -\frac{(\Psi_s(y))_y}{H}$ is background zonal current with variable topography, changes of which occur from north to south: $H = H(y)$, a $\tilde{\Psi}(x, y, t)$ are perturbations.

The equation for linear perturbations takes the form:

$$\left[\frac{\partial}{\partial t} + U \frac{\partial}{\partial x} \right] \left[\nabla_h^2 \tilde{\Psi} - \frac{H_y}{H} \Psi_y \right] + \Psi_x \beta^* = 0, \quad (5)$$

Where the role of β is fulfilled by β^* , the so-called ‘‘effective β ’’:

$$\beta^* = \beta - U_{yy} - \frac{f H_y}{H} + \frac{U_y H_y}{H}. \quad (6)$$

Then, for zonal wave perturbations of the form $\tilde{\Psi}(x, y, t) = \tilde{\Psi}(y) \exp(i k (x - c t))$, where k is zonal wavenumber, c is phase velocity of waves, we obtain a one-dimensional differential linear equation:

$$(U - c) \left[\Psi_{yy} - \frac{H_y}{H} \Psi_y - k^2 \tilde{\Psi} \right] + \beta^* \tilde{\Psi} = 0. \quad (7)$$

Further, with the standard replacement $\tilde{\Psi} = \sqrt{H} \varphi$, we eliminate the first derivative:

$$(U - c) \left[\varphi_{yy} - \left(k^2 + \frac{1}{4} \left(\frac{H_y}{H} \right)^2 - \frac{1}{2} \left(\frac{H_y}{H} \right)_y \right) \varphi \right] + \beta^* \varphi = 0. \quad (8)$$

Further, we assume that the model parameters change slowly in the transverse direction. Then, in the standard WKB approximation, setting $\varphi \sim \exp(i ly)$, where l is meridional wavenumber, taking into account the first Rhines approximation, we obtain the following dispersion relation for the phase velocity:

$$c^* = \frac{\omega}{k} = \frac{-\left(\beta - U_{yy} - \frac{f H_y}{H} + \frac{H_y U_y}{H}\right)}{k^2 + l^2} + U. \quad (9)$$

Dispersion expression (9) describes the propagation of barotropic Rossby waves with allowance for large-scale changes in depth H and in the presence of a zonal jet stream with a velocity U . Its novelty lies in the appearance of a new, additional fourth term in the numerator of the fraction.

Let us analyze the relative contribution of each term in the expression for β^* . Note, that the **first term** β and the **second** U_{yy} enter the expression for β^* with different signs. Effect of **the third term** in the numerator $\frac{f H_y}{H}$ can be defined as follows: for a zonal ridge from its northern and southern sides, the ocean depth increases in the direction from its top. This means that on the north side of the ridge $H_y < 0$ (depth increases with decreasing y), and on the south side, on the contrary, $H_y > 0$. Since for the southern hemisphere $f < 0$, then on the north side $\left(-\frac{f H_y}{H}\right) > 0$, that is, the third term (taking into account the minus) enhances β -effect, and vice versa, reduces it from the south side. This is consistent with [2], that in the southern hemisphere, on the northern side of the ridge, with a meridional change in depth, topography enhances the β -effect, and the wave phase receives an additional western component, and, conversely, the topography weakens the β -effect from the southern side of the ridge, where the phase of the waves receives an eastern component. Input of **the fourth term** in the expression for β^* depends on the shape and location of the jet relative to the ridge.

To compare numerically the estimates of the contribution of the terms in expression (6) for β^* , consider various options for their parameterization.

3.2. Zonal flow

For the zonal flow U , we use the GLORYS12v1 reanalysis data, where both satellite and *in situ* data are assimilated (see Section 2). Fig. 1 shows the velocity field constructed with GLORYS12v1 data for the ACC region, as well as the spatial distributions of the first and second meridional derivatives that are used in the expression for β^* (see Inset). Note that fig. 1, *a* shows both positive and negative zonal velocities. In fact, the ACC, like any ocean current, meanders significantly. The formation of meanders leads to a change in the velocity vectors' directions and the presence of components with opposite signs. With a significant temporal and spatial averaging, this factor of variability is insignificant or completely leveled out. In fig. 1, *a*, the band where the averaged zonal velocities are most intense (> 40 cm/s) is located in the latitude range from 42° to 54° S. Also, the signs are opposing for the magnitudes of the first derivative U'_y in fig. 1, *b* and the second derivative U_{yy} of the velocity in fig. 1, *c*.

In this paper, we evaluate jointly the relative influence of three factors: β -effect, currents and topography. For this purpose, we will consider two models of the bottom topography, given by simple analytical functions that approximate the zonal ridge.

3.3. Bottom relief

3.3.1. Zonal oriented endless ridge with exponential slopes

An example of a ridge profile is shown in fig. 2. The bottom relief contains a ridge elongated zonally along 50° S. The meridional depth gradients are the same on both sides of the ridge. This topography option can be approximated by the following formula:

$$H(y) = \begin{cases} H_2 - H_1 \exp\left(-\frac{y+50}{l}\right), & -50^\circ \leq y < -40^\circ, \\ H_2 - H_1 \exp\left(\frac{y+50}{l}\right), & -60^\circ \leq y < -50^\circ, \end{cases} \quad (10)$$

where H_1 is maximum height of the ridge relative to the bottom, H_2 is the ocean depth.

Table 1

Estimation of the components of the dispersion equation (10) for models 1–4 (values are normalized to $10^{-11} \text{ m}^{-1}\text{s}^{-1}$)

Latitudes, °S	β	U_{yy}	$\frac{f H_y}{H}$	$\frac{H_y U_y}{H}$
	(1)	(2)	(3)	(4)
Model 1, $H_2 - H_1 = 500 \text{ m}$, $l = 370.5 \text{ km}$				
40	1.8	-2.8	-1.2	0.004
45	1.6	4.8	-6.9	-0.06
49.5	1.5	4.7	-97.0	-1.2
55	1.3	0.7	8.0	-0.06
60	1.1	1.1	1.6	0.003
Model 2, $H_2 - H_1 = 1000 \text{ m}$, $l = 387.8 \text{ km}$				
40	1.8	-2.8	-1.2	0.003
45	1.6	4.8	-6.0	-0.05
49.5	1.5	4.7	-59.0	-0.74
55	1.3	0.7	7.0	-0.06
60	1.1	1.1	1.6	0.003
Model 3, $H_2 - H_1 = 500 \text{ m}$, $l = 92.6 \text{ km}$				
47.5	1.5	-2.2	-6.3	-0.05
48	1.5	-2.1	-10.4	0.12
49.5	1.5	4.7	-115.0	-1.44
51	1.4	-7.3	45.4	-0.95
52.5	1.4	-6.7	6.8	0.07
Model 4, $H_2 - H_1 = 1000 \text{ m}$, $l = 97.0 \text{ km}$				
47.5	1.5	-2.2	-6.0	-0.05
48	1.5	-2.1	-9.6	0.11
49.5	1.5	4.7	-90.0	-1.13
51	1.4	-7.3	39.0	-0.82
52.5	1.4	-6.7	6.4	0.06

To obtain the estimates, we considered two variants of the exponential profile, when the ridge “width” was 2220 km (20° along the meridian) and 555 km (5°), and for each of them, there were also two variants of the minimum depth above the ridge top ($H_2 - H_1$), 500 and 1000 m (fig. 2, *b*), that is, in total four models of ridges. The functions’ parameters (model 1, fig. 2, *b*) followed the condition that the depth reaches 4300 m at a distance of 1110 km from the summit. In model 2, the depth above the ridge top was 1000 m, and in models 3 and 4, the same 500 and 1000 m, but here we study abrupt depth increase in the direction away from the ridge top, i. e., the depth becomes equal to 4300 m at a distance of 277.5 km (2.5°). For the open ocean, the typical bottom slopes are 10^{-3} – 10^{-1} . In our examples (fig. 2), the slopes range from 0.9×10^{-2} до 2.7×10^{-2} .

Contribution estimates of various terms in the expression for β^* are presented in table 1 (terms are numbered). According to the table, the largest contribution to β^* is from topography, which is the third term: $\frac{f H_y}{H}$. In the vicinity of the ridge top, for all considered exponential relief forms, the third term exceeded the values of all the others more than by order of magnitude. Consequently, it is the topography that contributes the most to the phase velocity of Rossby waves, increasing β -effect in the southern hemisphere to the north of the ridge and weakening it to the south, as shown in section 3.1. According to the table, relative input of other terms is inferior to the contribution of the third term for all studied exponential relief profiles (fig. 2, see Inset).

3.3.2. Zonal oriented endless ridge with Gaussian slopes

Fig. 3 shows the vertical relief profiles in the form of a Gaussian:

$$H(y) = \begin{cases} H_2 - H_1 \exp\left(-\frac{(y+50)^2}{\sigma^2}\right), & -60^\circ \leq y \leq -40^\circ. \end{cases} \quad (11)$$

Table 2

**Estimation of the components of the dispersion equation (10) for models 5–8
(values are normalized to $10^{-11} \text{ m}^{-1}\text{s}^{-1}$)**

Latitudes, °S	β	U_{yy}	$\frac{f H_y}{H}$	$\frac{H_y U_y}{H}$
	(1)	(2)	(3)	(4)
Model 5, $H_2 - H_1 = 500 \text{ m}$, $\sigma = 641 \text{ km}$				
40	1.8	-2.8	-2.5	0.008
45	1.6	4.8	-20.0	-0.17
49.5	1.5	4.7	-22.0	-0.28
55	1.3	0.7	23.0	-0.19
60	1.1	1.1	3.4	0.006
Model 6, $H_2 - H_1 = 1000 \text{ m}$, $\sigma = 457 \text{ km}$				
40	1.8	-2.8	-2.4	0.007
45	1.6	4.8	-16.0	-0.14
49,5	1.5	4.7	-9.6	-0.12
55	1.3	0.7	19.0	-0.16
60	1.1	1.1	3.2	0.005
Model 7, $H_2 - H_1 = 500 \text{ m}$, $\sigma = 160 \text{ km}$				
47.5	1.5	-2.2	-14.8	-0.11
48	1.5	-2.1	-28.3	0.32
49.5	1.5	4.7	-173.4	-2.16
51	1.4	-7.3	117.2	-2.46
52.5	1.4	-6.7	14.9	0.15
Model 8, $H_2 - H_1 = 1000 \text{ m}$, $\sigma = 164 \text{ km}$				
47.5	1.5	-2.2	-13.0	-0.1
48	1.5	-2.1	-25.5	0.29
49.5	1.5	4.7	-100.7	-1.25
51	1.4	-7.3	88.6	-1.86
52.5	1.4	-6.7	14.0	0.14

In models 5–8 (fig. 3, see Inset), we set the relief parameters in the same way as in models 1–4. A comparative analysis of the terms for this ridge approximation showed that the contribution of the third term to β^* is dominant, i. e., from the north of the ridge, the topography increases the β -effect, and from the south, vice versa. The results are shown in table 2.

Fig. 1, c and tables 1 and 2 show that the values U_{yy} locally may exceed β . This means that in the studied water area, the current shift is comparable to the β -effect and can overpower its influence, so that the phase of the waves can change to the opposite and, consequently, the waves will propagate to the east. The authors previously considered this effect in the ACC region and compared the contribution of the β -effect and shear current to wave propagation [10] with the current velocities calculated from altimetry data.

It can also be seen from tables 1 and 2 that, for flat slopes, the meridional shear gradient of the zonal current can overpower the topography contribution locally. However, in general, the contribution of topography (the third term) is dominant for the zonal ocean ridge.

3.3.3. Parametrization of a Shear Flow and Corresponding Estimation of Its Contribution

Section 3.2 shows the estimates of the flow calculated from the reanalysis data. Let us consider the combined effect of zonal jet flow and topography based on simple flow models in the form of analytical functions.

Let the current be directed to the east and the profile of its velocity is described by a parabola with a top at 50°S with a decrease to the north and south of the main stream, so that at 40°S and 60°S the flow velocity is zero:

$$U = U_0 \frac{(10^2 - (y + 50)^2)}{10^2}, \text{ variable } y \text{ varies from } 40^\circ\text{S up to } 60^\circ\text{S. Let the amplitude } U_0 = 1 \text{ m/s. Therefore,}$$

$$U_y = U_0 \frac{(-2(y + 50))}{111.2} \cdot 10^{-4} \text{ (c}^{-1}\text{) and } U_{yy} = -1.62 \cdot 10^{-12} \text{ (m}^{-1}\text{s}^{-1}\text{). Let us consider another parameterization of the}$$

shear flow: now let the eastward flow be approximated by the Gaussian $U = U_0 \exp\left(-\frac{(y-b)^2}{2a^2}\right)$, where $U_0 = 1$ m/s, b is the center of the velocity of the background flow, a is the jet width, $y = b \pm a$ is the inflection point. So $U_y = -\frac{(y-b)}{a^2} U_0 \exp\left(-\frac{(y-b)^2}{2a^2}\right)$, and $U_{yy} = \frac{(y-b)^2 - a^2}{a^4} U_0 \exp\left(-\frac{(y-b)^2}{2a^2}\right)$. Let $b = -50^\circ$, $a = 2^\circ$. With a jet width of 2 meridian degrees (222 km) on the streamline (maximum speed) at $y = -50^\circ$, we get: $U_{yy} = -\frac{1}{a^2} = -2.02 \cdot 10^{-11} < 0$, that is, the flow again increases the influence β -effect.

Apparently, real fluxes cannot be adequately approximated by the presented functions, since it is impossible to account for numerous factors, temporal variability, barotropic and baroclinic instability, the occurrence of meanders, and many other effects that exist in nature. However, the following is obvious: the contribution of the shear current to the propagation of Rossby waves may differ for the same water area, both strengthening, weakening, or even suppression of the β -effect can occur in the same region, and this essentially depends on the shape of the jet, that is, on the sign of U_{yy} .

Fig. 1 uses GLORYS12v1 data and shows that the values U_{yy} can be both negative and positive in the ACC region. In the latter case, the shear flow is opposed to the β -effect and, as can be seen from tables 1 and 2, in many cases, the flow prevails and overpowers the β -effect. We discovered this feature earlier when analyzing altimetry data in the ACC region [10].

A new approximation can be formulated (by analogy with the Rhines approximation [31]), as the key outcome of the comparison. Since the ratio of the fourth column of the table to the third is the Rossby number, this approximation appears to read: for small Rossby numbers, the last term in the dispersion relation can be neglected.

3.3.4. Verification

The question arises: to what extent are the obtained estimates applicable to the real ocean? Let us consider the water area located above the Australian-Antarctic ridge within the boundaries, which in terms of parameters satisfies our models well (fig. 4, *a*; see Inset). Another example is the zoned South Scotia Ridge (fig. 5, *a*; see Inset). In some areas of these ridges, the considered analytical models approximate the relief well. Slopes H_y/H vary in the range $2.70 \times 10^{-2} \div 1.8 \times 10^{-1} \text{ m}^{-1}$, so that the contribution of the third term to the expression for β^* is equal $3.2 \times 10^{-6} \div 2.3 \times 10^{-5} \text{ s}^{-1} \text{ m}^{-1}$.

There are several jets of ACC in the band of latitudes from 40° to 60°S . We considered the zonal component of the current and its two derivatives for the studied water areas, calculated with the GLORYS12v1 product. Fig. 4 (*b-d*) and 5 (*b-d*) show that zonal velocities in water areas can reach 50 cm/s for the Australian-Antarctic ridge and 30 cm/s for the South Scotia Ridge. Apparently, both positive and negative flow rates are present. Comparison of the second term in the tables U_{yy} with the values of the third as $\frac{f H_y}{H}$ shows that for the analyzed water areas the topographic factor prevails.

4. Conclusions and discussion

In this work, we offer a generalized dispersion relation for linear Rossby waves on a zonal jet stream taking into account the influence of bottom topography and shear zonal flow. We introduce an additional term into the dispersion relation to represent the combined effect of topography and meridional variability of the background flow. The effects of the differential rotation of the Earth, topography, and shear flow on Rossby waves are studied. We obtained the estimates for model zonal ridges with the GLORYS12v1 product current velocities for the area limited to $40\text{--}60^\circ\text{S}$, $80\text{--}120^\circ\text{E}$. There is the Australian-Antarctic ridge, and several ACC jets are located in the area. We studied a zonally oriented ridge as a model topographic structure, the topography of which is approximated by an exponent or a Gaussian with two different parameters.

The main results of the work are as follows. When the Earth's rotation, topography variability, and background current are taken into account together, an additional term $\frac{U_y H_y}{H}$, appears in the dispersion relation, which appears to be insignificant. Its ratio to the term responsible for the change in topography is the Rossby number. Thus, it is

possible to introduce a new approximation into scientific circulation as follows: at low Rossby numbers in the dispersion relation, the additional term corresponding to the combined effect of topography and the meridional variability of the background flow is insignificant.

It is shown that, locally, the contribution of the shear flow can overpower the effect of the β -parameter. Qualitative and quantitative estimates obtained earlier from altimetry indicate a similar result (see [10]). Also, a comparison of the contributions of topography and flow shows that the topographic factor prevails in the given problem statement. In this case, depending on the location and shape of the jet, the flow can both weaken and enhance the β -effect. However, the topographic factor in the dispersion equation is the main one. Thus, on the northern side of the zonal ridge located in the southern hemisphere, topography enhances the β -effect, and on the southern side, it weakens.

Thus, in the dispersion relation, rotation and topography compete, on the one hand, and the velocity gradient and topography, on the other. A new player appears in our problem statement: $\frac{H_y U_y}{H}$, and it shifts everything in the direction of rotation. This means that topography and rotation always dominate. In other words, even for such strong jet currents as ACC, the combined effect of topography and meridional variability of the background current is much inferior to the combined effect of differential Earth rotation and topography. So, an attempt to take into account an additional factor in the form of the joint influence of the variability of the flow and topography is rather fruitless, and, therefore, the isolines of the traditional ratio $\frac{f}{H}$ work quite well in various parts of the ocean.

The analysis performed allows us to formulate a new approximation, by analogy with the Rhines approximation [31]: at low Rossby numbers, the last term in the dispersion relation reflecting the combined effect of topography and meridional variability of the background flow is insignificant.

5. Funding

The research was funded by RFBR, project number 20–05–00066.

Литература

1. *Незлин М.В.* Солитоны Россби (Экспериментальные исследования и лабораторная модель природных вихрей типа Большого Красного Пятна Юпитера) // *Успехи физических наук.* 1986. Т. 150, № 9. С. 3–60. doi: 10.3367/UFNr.0150.198609a.0003
2. *Ле Блон П., Майсек Л.* Волны в океане В 2-х ч. / Пер. с англ. М.: Мир, 1981. 846 с.
3. *Veronis G.* Rossby waves with bottom topography // *J. Mar. Res.* 1966. V. 24, N 3. P. 338–349.
4. *Rhines P.B.* Edge-, bottom-, and Rossby waves in a rotating stratified fluid // *Geophys. Fluid Dyn.* 1970. V. 1, N 3–4. P. 273–302. doi: 10.1080/03091927009365776
5. *Killworth P.D., Blundell J.R.* Long extratropical planetary wave propagation in the presence of slowly varying mean flow and bottom topography. Part I: The Local Problem // *J. Phys. Oceanogr.* 2003. V. 33, N 4. P. 784–801. doi: 10.1175/1520-0485(2003)33<784:LEPWPI>2.0.CO;2
6. *Killworth P.D., Blundell J.R.* Planetary wave response to surface forcing and to instability in the presence of mean flow and topography // *J. Phys. Oceanogr.* 2007. V. 37. P. 1297–1320. doi: 10.1175/JPO3055.1
7. *Charney J.G., Flierl G.R.* Oceanic analogues of large-scale atmospheric motions // *Evolution of Physical Oceanography* / Eds. B.A. Warren and C. Wunsch, Chapter 18. Cambridge, Massachusetts: MIT Press, 1981. P. 504–548.
8. *Bobrovich A.V., Reznik G.M.* Planetary waves in a stratified ocean of variable depth. Part 2. Continuously stratified ocean // *J. Fluid. Mech.* 1999. V. 388. P. 147–169. doi: 10.1017/S0022112099004863
9. *Каменкович В.М., Монин А.С.* Физика океана. Т. 2: Гидродинамика океана. М.: Наука, 1978. 435 с.
10. *Гневнышев В.Г., Фролова А.В., Кубряков А.А., Собко Ю.В., Белоненко Т.В.* Взаимодействие волн Россби со струйным потоком: основные уравнения и их верификация для антарктического циркумполярного течения // *Изв. РАН. Физ. атм. и океана.* 2019. Т. 55, № 5. С. 39–50.
11. *Педлоски Дж.* Гидрофизическая гидродинамика / Пер. с англ. В 2 т. М.: Мир, 1984. 398 с. (т. 1), 416 с. (т. 2).
12. *La Casce J.H.* The prevalence of oceanic surface modes // *Geophys. Res. Lett.* 2017. V. 44. P. 11097–11105. doi: 10.1002/2017GL075430
13. *Brink K.H., Pedlosky J.* Rossby Waves with Continuous Stratification and Bottom Friction // *J. Phys. Oceanogr.* 2018. V. 48, N 9. P. 2209–2219. doi: 10.1175/JPO-D-18-0070.1
14. *Killworth P.D., Blundell J.R.* The dispersion relation for planetary waves in the presence of mean flow and topography. Part I: Analytical theory and one-dimensional examples // *J. Phys. Oceanogr.* 2004. V. 34, N12. P. 2692–2711. doi: 10.1175/JPO2635.1

15. Killworth P.D., Blundell J.R. The dispersion relation for planetary waves in the presence of mean flow and topography. Part II: two-dimensional examples and global results // *J. Phys. Oceanogr.* 2005. V. 35, N 11. P. 2110–2133.
16. Гилл А. Динамика атмосферы и океана. В 2 т. / Пер. с англ. М.: Мир, 1986. 396 с. (т. 1), 415 с. (т. 2).
17. Chelton D.B., de Szoeke R.A., Schlax M.G., El Naggar K., Siwertz N. Geographical variability of the first baroclinic Rossby radius of deformation // *J. Phys. Oceanogr.* 1998. V. 28, N 3. P. 433–460.
doi: 10.1175/1520-0485(1998)028<0433:GVOTFB>2.0.CO;2
18. Chelton D.B., Schlax M.G., Samelson R.M. Global observations of nonlinear mesoscale eddies // *Prog. Oceanogr.* 2011. 91, 167–216. doi: 10.1016/j.pocean.2011.01.002
19. Тараканов Р.Ю. Структура крупномасштабной циркуляции антарктических вод: автореф. дис. на соиск. учен. степ. док. физ.-мат. наук (25.00.28) / Роман Юрьевич Тараканов; Институт океанологии им. П.П. Ширшова. Москва, 2015. 42 с.
20. Knauth J.A., Garfield N. Introduction to physical oceanography. Waveland Press, 2016. 310 p.
21. Zyryanov V.N. Topographic eddies in a stratified ocean // *Regular and chaotic dynamics.* 2006. V. 11, N 4. P. 491–521.
doi: 10.1070/RD2006v011n04ABEH000367
22. Nowlin W.D., Klinck J.M. The physics of the Antarctic circumpolar current // *Rev. Geophys.* 1986. V. 24, N 3. P. 469–491. doi: 0.1029/RG024i003p00469
23. Smith K.S., Marshall J. Evidence for enhanced eddy mixing at middepth in the Southern Ocean // *J. Phys. Oceanogr.* 2009. V. 39. P. 50–69. doi: 10.1175/2008JPO3880.1
24. Phillips H.E., Rintoul S.R. Eddy variability and energetics from direct current measurements in the Antarctic Circumpolar Current south of Australia // *J. Phys. Oceanogr.* 2000. V. 30, N 12. P. 3050–3076.
doi: 10.1175/1520-0485(2000)030<3050: EVAEFD>2.0.CO;2
25. Morrow R., Le Traon P.-Y. Recent advances in observing mesoscale ocean dynamics with satellite altimetry // *Adv. Spa. Res.* 2012. V. 50, N8. P. 1062–1076. doi: 10.1016/j.asr.2011.09.033
26. Donohue K.A., Watts D.R., Hamilton P., Leben R., Kennelly M. Loop current eddy formation and baroclinic instability // *Dyn. Atmos. Oceans.* 2016. V. 76, Part 2. P. 195–216. doi: 10.1016/j.dynatmoce.2016.01.004
27. Marshall D. Topographic steering of the Antarctic Circumpolar Current // *J. Phys. Oceanogr.* 1995. V. 25, N 7. P. 1636–1650. doi: 10.1175/1520-0485(1995)025<1636: TSOTAC>2.0.CO;2
28. Ruan X., Thompson A.F., Flexas M.M., Sprintall J. Contribution of topographically generated submesoscale turbulence to Southern Ocean overturning // *Nature Geoscience.* 2017. V. 10, N 11. P. 840–845. doi: 10.1038/ngeo3053
29. Thompson A.F. The atmospheric ocean: eddies and jets in the Antarctic Circumpolar Current // *Philosophical Transactions of the Royal Society of London A: Mathematical, Physical and Engineering Sciences.* 2008. V. 366, N 1885. P. 4529–4541. doi: 10.1098/rsta.2008.0196
30. Белоненко Т.В., Захарчук Е.А., Фукс В.Р. Градиентно-вихревые волны в океане. СПб.: Изд-во СПбГУ, 2004. 215 с.
31. Rhines P.B. Slow oscillation in an ocean of varying depth. Part 1. Abrupt topography // *J. Fluid Mech.* 1969. V. 37, N 1. P. 161–189. doi: 10.1017/S0022112069000474

References

1. Nezlin M.V. Rossby solitons (Experimental investigations and laboratory model of natural vortices of the Jovian Great Red Spot type). *Sov. Phys. Usp.* 1986, 29, 807–842. doi: 10.1070/PU1986v029n09ABEH003490
2. LeBlond P., Mysak L.A. Waves in the Ocean. Elsevier Scientific Publishing Company, 1977. 602 p.
3. Veronis G. Rossby waves with bottom topography. *J. Mar. Res.* 1966, 24, 3, 338–349.
4. Rhines P.B. Edge-, bottom-, and Rossby waves in a rotating stratified fluid. *Geophys. Fluid. Dyn.* 1970, 1, 3–4, 273–302.
5. Killworth P.D., Blundell J.R. Long extratropical planetary wave propagation in the presence of slowly varying mean flow and bottom topography. Part I: The Local Problem. *J. Phys. Oceanogr.* 2003, 33, 4, 784–801.
doi: 10.1175/1520-0485(2003)33<784: LEPWPI>2.0.CO;2
6. Killworth P.D., Blundell J.R. Planetary wave response to surface forcing and to instability in the presence of mean flow and topography. *J. Phys. Oceanogr.* 2007, 37, 1297–1320. doi: 10.1175/JPO3055.1
7. Charney J.G., Flierl G.R. Oceanic analogues of large-scale atmospheric motions. *Evolution of Physical Oceanography.* Eds. B.A. Warren, C. Wunsch. Chapter 18. MIT Press, Cambridge, Massachusetts, 1981, P. 504–548.
8. Bobrovich A.V., Reznik G.M. Planetary waves in a stratified ocean of variable depth. Part 2. Continuously stratified ocean. *J. Fluid Mech.* 1999, 388, 147–169. doi: 10.1017/S0022112099004863
9. Kamen'kovich V.M., Monin A.S. Physics of the ocean. V. 2.: Hydrodynamics of ocean. М., Nauka, 1978. 435 p. (in Russian).
10. Gnevyshev V.G., Frolova A.V., Kubryakov A.A., Sobko Yu.V., Belonenko T.V. Interaction of Rossby waves with a jet stream: basic equations and their verification for the Antarctic circumpolar current. *Izv. Atmos. Oceanic Phys.* 2019, 55, 5, 412–422. doi: 10.1134/S0001433819050074

11. Pedlosky J. Geophysical Fluid Dynamics. Berlin, Springer, 1979. 624 p.
12. La Casce J.H. The prevalence of oceanic surface modes. *Geophys. Res. Lett.* 2017, 44, 11097–11105. doi: 10.1002/2017GL075430
13. Brink K.H., Pedlosky J. Rossby Waves with Continuous Stratification and Bottom Friction. *J. Phys. Oceanogr.* 2018, 48, 2209–2219. doi: 10.1175/JPO-D-18-0070.1
14. Killworth P.D., Blundell J.R. The dispersion relation for planetary waves in the presence of mean flow and topography. Part I: Analytical theory and one-dimensional examples. *J. Phys. Oceanogr.* 2004, 34, 12, 2692–2711. doi: 10.1175/JPO2635.1
15. Killworth P.D., Blundell J.R. The dispersion relation for planetary waves in the presence of mean flow and topography. Part II: two-dimensional examples and global results. *J. Phys. Oceanogr.* 2005, 35, 11, 2110–2133.
16. Gill A.E. Atmosphere–Ocean Dynamics. Academic Press. 1982. 662 p.
17. Chelton D.B., de Szoeke R.A., Schlax M.G., El Naggar K., Siefert N. Geographical variability of the first-baroclinic Rossby radius of deformation. *J. Phys. Oceanogr.* 1998, 28, 3, 433–460. doi: 10.1175/1520-0485(1998)028<0433:GVOTFB>2.0.CO;2
18. Chelton D.B., Schlax M.G., Samelson R.M. Global observations of nonlinear mesoscale eddies. *Prog. Oceanogr.* 2011, 91, 167–216. doi: 10.1016/j.pocean.2011.01.002
19. Tarakanov R. Yu. Doctoral Dissertation in Physics and Mathematics. Institute of Oceanology, Russian Academy of Sciences, Moscow, 2015. (in Russian).
20. Knauss J.A., Garfield N. Introduction to physical oceanography. Waveland Press, 2016. 310 p.
21. Zyryanov V.N. Topographic eddies in a stratified ocean. *Regular and Chaotic Dynamics.* 2006, 11, 4, 491–521. doi: 10.1070/RD2006v011n04ABEH000367
22. Nowlin W.D., Klinck J.M. The physics of the Antarctic circumpolar current. *Rev. Geophys.* 1986, 24, 3, 469–491. doi: 10.1029/RG024i003p00469
23. Smith K.S., Marshall J. Evidence for enhanced eddy mixing at middepth in the Southern Ocean. *J. Phys. Oceanogr.* 2009, 39, 50–69. doi: 10.1175/2008JPO3880.1
24. Phillips H.E., Rintoul S.R. Eddy variability and energetics from direct current measurements in the Antarctic Circumpolar Current south of Australia. *J. Phys. Oceanogr.* 2000, 30, 12, 3050–3076. doi: 10.1175/1520-0485(2000)030<3050:EVAEFD>2.0.CO;2
25. Morrow R., Le Traon P.-Y. Recent advances in observing mesoscale ocean dynamics with satellite altimetry. *Adv. Spa. Res.* 2012, 50, 1062–1076. doi: /10.1016/j.asr.2011.09.033
26. Donohue K.A., Watts D.R., Hamilton P., Leben R., Kennelly M. Loop current eddy formation and baroclinic instability. *Dyn. Atmos. Oceans.* 2016, 76, part 2, 195–216. doi: 10.1016/j.dynatmoce.2016.01.004
27. Marshall D. Topographic steering of the Antarctic Circumpolar Current. *J. Phys. Oceanogr.* 1995, 25, 7, 1636–1650. doi: 10.1175/1520-0485(1995)025<1636:TSOTAC>2.0.CO;2
28. Ruan X., Thompson A.F., Flexas M.M., Sprintall J. Contribution of topographically generated submesoscale turbulence to Southern Ocean overturning. *Nature Geoscience.* 2017, 10, 11, 840–845. doi: 10.1038/ngeo3053
29. Thompson A.F. The atmospheric ocean: eddies and jets in the Antarctic Circumpolar Current. *Philosophical Transactions of the Royal Society of London A: Mathematical, Physical and Engineering Sciences.* 2008, 366, 1885, 4529–4541. doi: 10.1098/rsta.2008.0196
30. Belonenko T.V., Zakharchuk E.A., Fuks V.R. Gradient-vortex waves in the ocean. *St. Petersburg, Izdatelstvo SPbGU.* 2004. 215 p. (in Russian).
31. Rhines P.B. Slow oscillation in an ocean of varying depth. Part 1. Abrupt topography. *J. Fluid. Mech.* 1969, 37, 1, 161–189. doi: 10.1017/S0022112069000474

К статье *Гневышев В.Г., Фролова А.В., Колдунов А.В., Белоненко Т.В.* Топографический эффект для волн Россби на зональном сдвиговом потоке
Gnevyshev V.G., Frolova A.V., Koldunov A.V., Belonenko T.V. Topographic effect for Rossby waves on a zonal shear flow

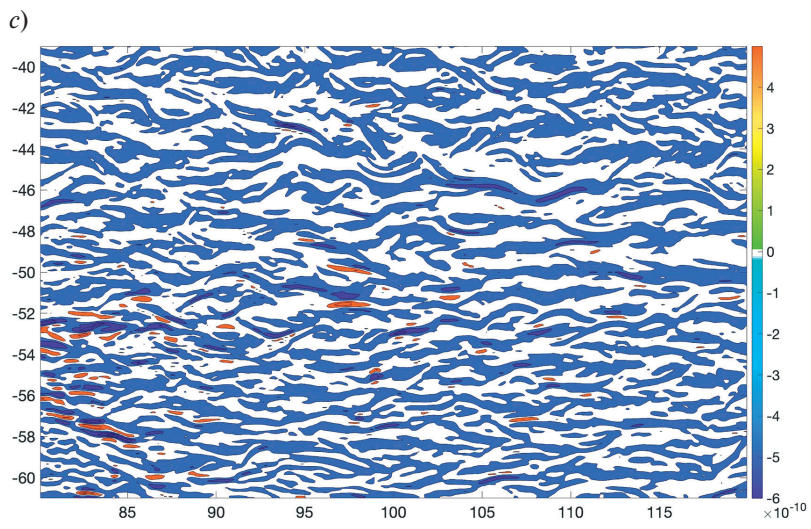
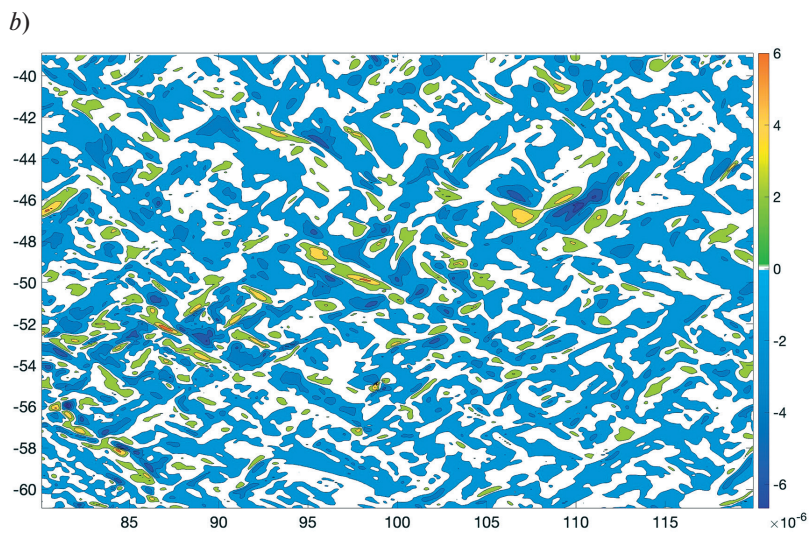
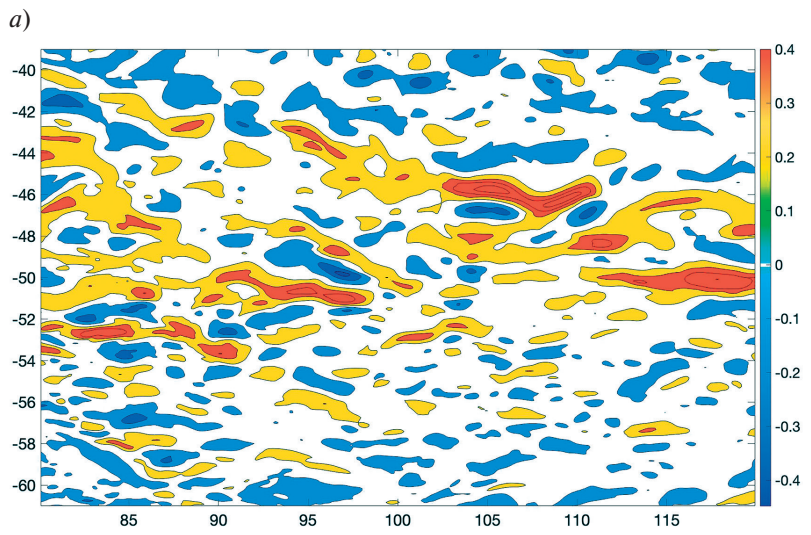


Fig. 1. Mean zonal flow velocities U (m / s) based on the GLORYS12v1 data (a), U_y (s^{-1}) (b) and U_{yy} ($m^{-1}s^{-1}$) (c). Averaging over the period 01–31.11.2018.

К статье *Гневышев В.Г., Фролова А.В., Колдунов А.В., Белоненко Т.В.* Топографический эффект для волн Россби на зональном сдвиговом потоке
Gnevyshev V.G., Frolova A.V., Koldunov A.V., Belonenko T.V. Topographic effect for Rossby waves on a zonal shear flow

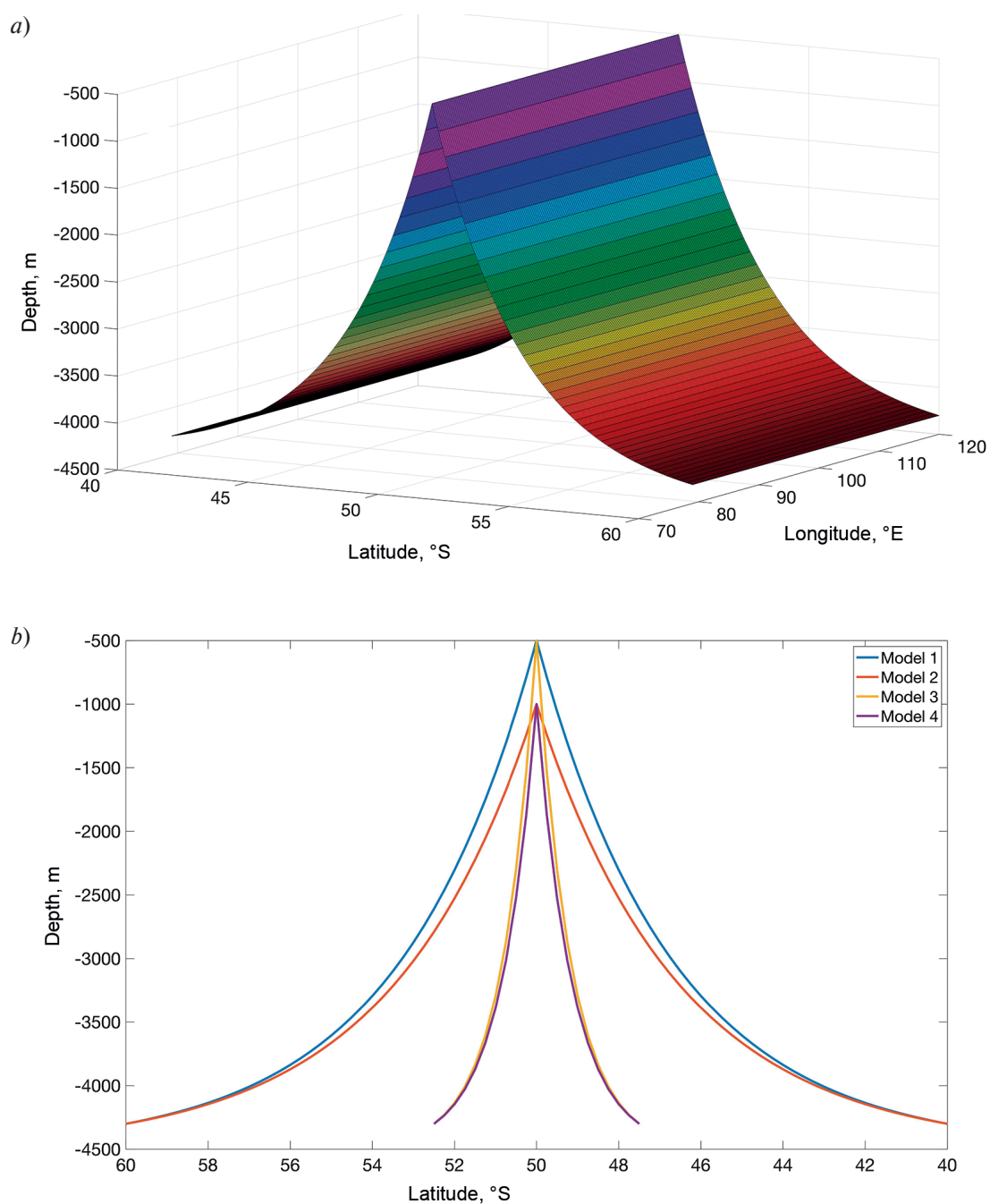


Fig. 2. Examples of the exponential relief profiles (10), for a ridge along 50°S with a depth above the ridge $H_2 - H_1 = 500$ m (model 1, $l = 370.5$ km). The vertical axis shows negative values for depth (m) (a). Vertical topography profiles on the models 1–4 (b).

К статье *Гневышев В.Г., Фролова А.В., Колдунов А.В., Белоненко Т.В.* Топографический эффект для волн Россби на зональном сдвиговом потоке
Gnevyshev V.G., Frolova A.V., Koldunov A.V., Belonenko T.V. Topographic effect for Rossby waves on a zonal shear flow

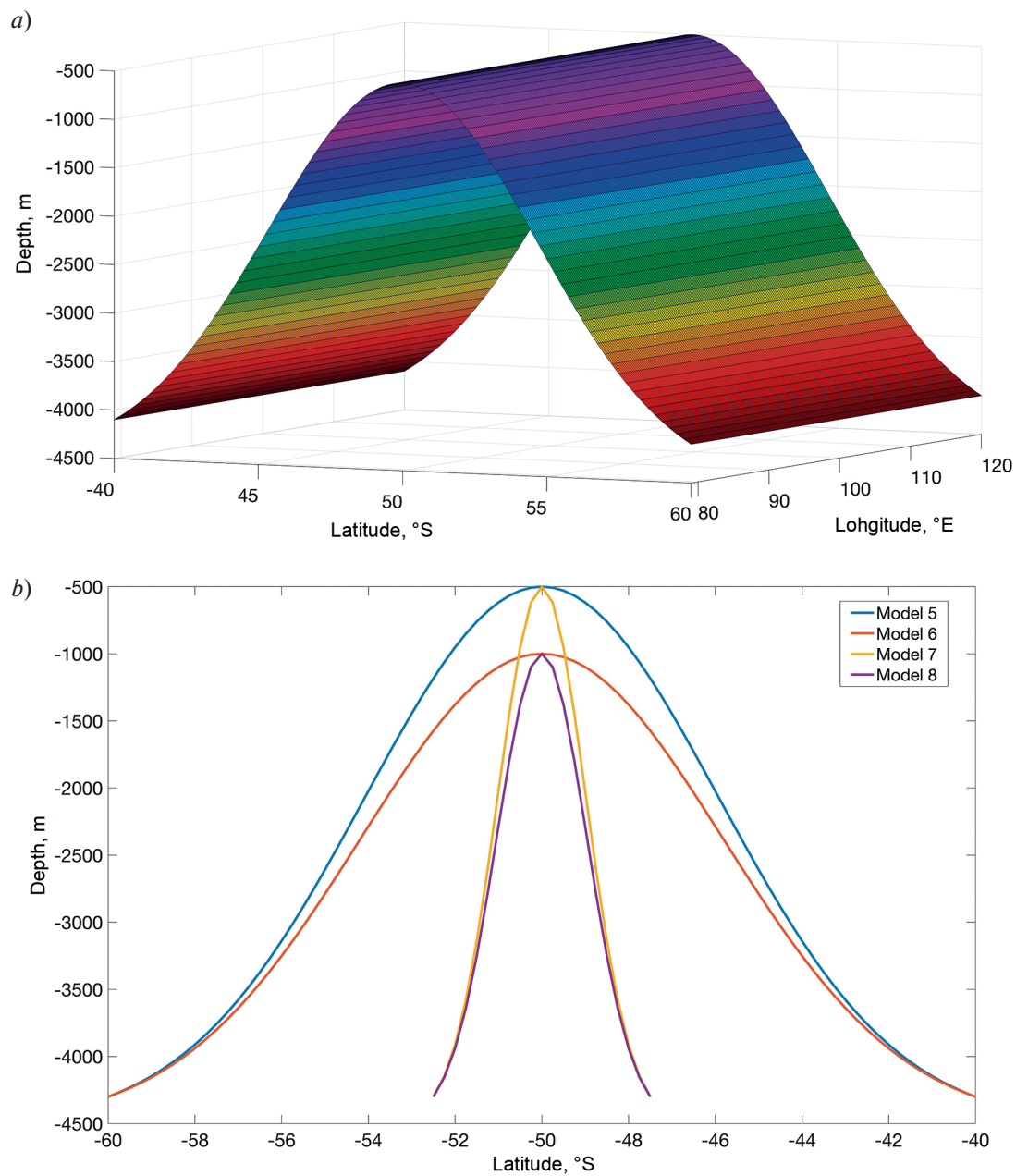
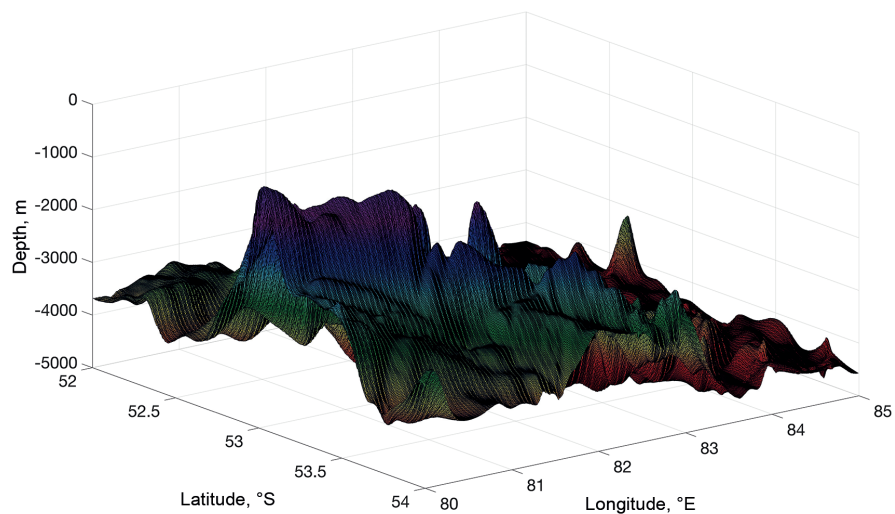


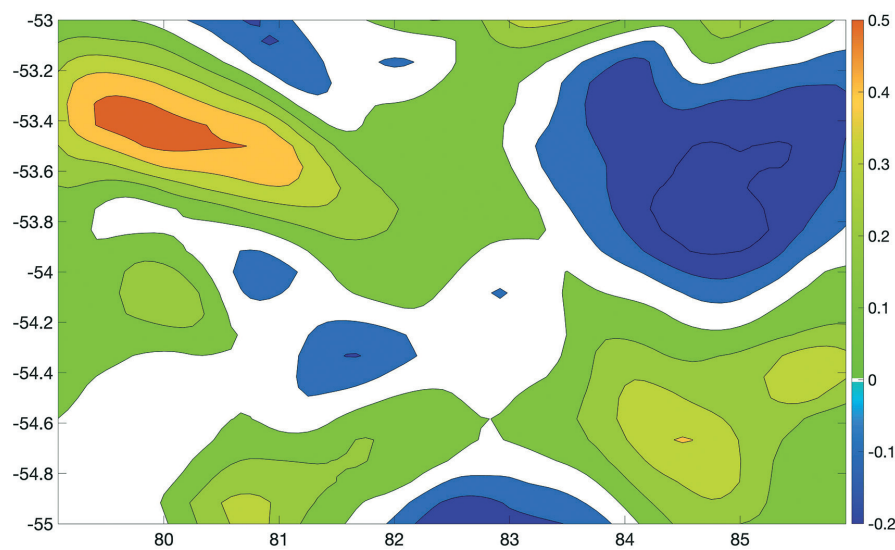
Fig. 3. Examples of the topography profiles (11), for a ridge along 50°S with a depth above the ridge $H_2 - H_1 = 500$ m (a). Vertical topography profiles for the models 5–8 (b).

К статье *Гневышев В.Г., Фролова А.В., Колдунов А.В., Белоненко Т.В.* Топографический эффект для волн Россби на зональном сдвиговом потоке
Gnevyshev V.G., Frolova A.V., Koldunov A.V., Belonenko T.V. Topographic effect for Rossby waves on a zonal shear flow

a)



b)



c)

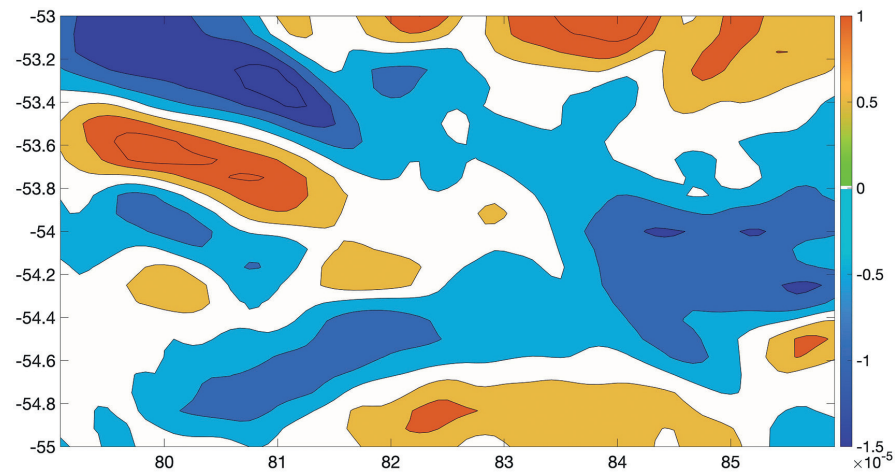


Fig. 4. Bottom topography according to GEBCO for part of the Australian–Antarctic Discordance (a); mean zonal flow velocities U (m/s) based on the GLORYS12v1 data (b), U_y (s^{-1}) (c) and U_{yy} ($m^{-1}s^{-1}$) (d). The abscissa axis shows longitudes, and the ordinate axis shows latitudes. The averaging is over the period 01–31.11.2018.

К статье *Гневышев В.Г., Фролова А.В., Колдунов А.В., Белоненко Т.В.* Топографический эффект для волн Россби на зональном сдвиговом потоке
Gnevyshev V.G., Frolova A.V., Koldunov A.V., Belonenko T.V. Topographic effect for Rossby waves on a zonal shear flow

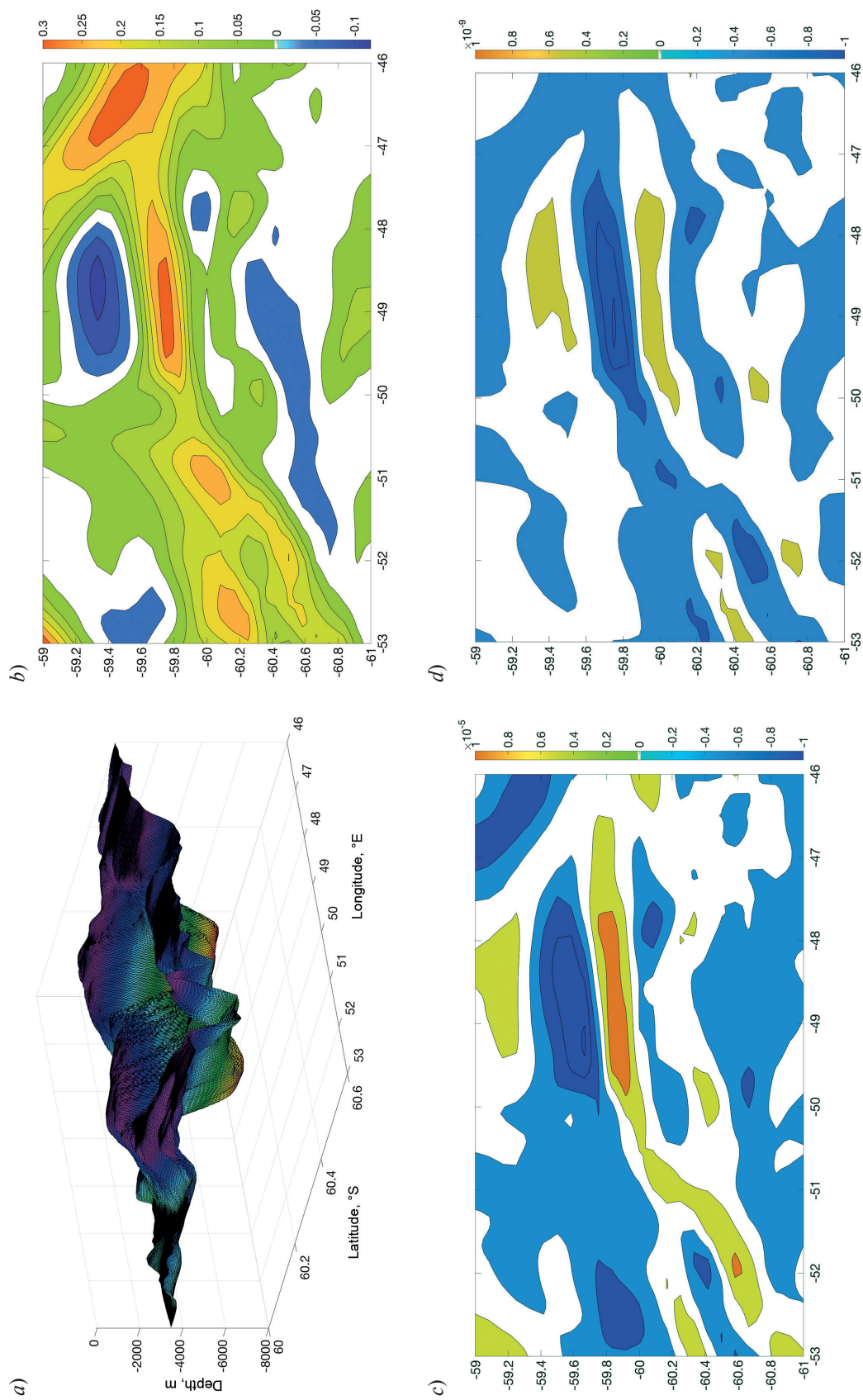


Fig. 5. Bottom topography according to GEBCO for part of the South Scotia Ridge (a); mean zonal flow velocities U (m / s) based on the GLORYS12v1 data (b), U_y (s^{-1}) (c) and U_x ($m^{-1}s^{-1}$) (d). The abscissa axis shows longitudes, and the ordinate axis shows latitudes. The averaging is over the period 01 – 31.11.2018.